Phase diagram and incommensurate antiferroelectric structure in (Pb11.5 x La x)(Zr0.42Sn0.40Ti0.18)O3 ceramics discovered by band-to-band optical transitions

X. J. Ding, L. P. Xu, Z. G. Hu, X. F. Chen, G. S. Wang, X. L. Dong, and J. H. Chu

Citation: Applied Physics Letters **105**, 131909 (2014); doi: 10.1063/1.4897357
View online: http://dx.doi.org/10.1063/1.4897357
View Table of Contents: http://scitation.aip.org/content/aip/journal/apl/105/13?ver=pdfcov
Published by the AIP Publishing

Phase diagram and incommensurate antiferroelectric structure in $(Pb_{1-1.5x}La_x)(Zr_{0.42}Sn_{0.40}Ti_{0.18})O_3$ ceramics discovered by band-to-band optical transitions

X. J. Ding (丁小娟),[1] L. P. Xu (徐丽萍),[1] Z. G. Hu (胡志高),[1,a)] X. F. Chen (陈学峰),[2] G. S. Wang (王根水),[2] X. L. Dong (董显林),[2] and J. H. Chu (褚君浩)[1]
[1]*Key Laboratory of Polar Materials and Devices, Department of Electronic Engineering, East China Normal University, Ministry of Education, Shanghai 200241, China*
[2]*Key Laboratory of Inorganic Functional Materials and Devices, Shanghai Institute of Ceramics, Chinese Academy of Sciences, Shanghai 200050, China*

(Received 29 July 2014; accepted 24 September 2014; published online 3 October 2014)

Optical properties and phase transitions of $(Pb_{1-1.5x}La_x)(Zr_{0.42}Sn_{0.40}Ti_{0.18})O_3$ (PLZST 100*x*/42/40/18) ceramics with different compositions have been investigated by temperature dependent spectroscopic ellipsometry. Two interband critical points (E_{cp1} and E_{cp2}) located at about 3.9 and 5.1 eV can be obtained by fitting standard line shapes to the second derivatives of the complex dielectric functions. Based on the band-to-band transitions, the phase diagram of PLZST ceramics can be well presented. Moreover, a peculiar incommensurate antiferroelectric state has been found to exist above the temperature of the normal commensurate antiferroelectric tetragonal structure. It can be stable below Curie temperature, evolving slowly with decreasing temperature towards the commensurate structure, which is due to strong pinning of incommensurate domain walls. The phenomena can result from a competition between ferroelectric ordering and antiferroelectric ordering caused by the lanthanum modification. © *2014 AIP Publishing LLC*. [http://dx.doi.org/10.1063/1.4897357]

In the past few decades, extensive studies of the complex Pb-based ABO_3 perovskite materials have been performed due to the excellent properties (ferroelectric, antiferroelectric, piezoelectric, and pyroelectric) obtained in the compositions close to morphotropic phase boundary (MPB).[1–4] Lead zirconate titanate (PZT) system as a typical perovskite material possesses unique properties, such as double hysteresis, large strain, considerable pyroelectric coefficient, and huge electrocaloric effect, which make them as potential materials in applications of high-energy-storage capacitors, high-strain transducers or actuators, infrared detectors, and cooling devices.[1] Lanthanum (La) modification in the A-cation was often used to improve physical properties, such as suppression of long-range ferroelectric order and enhancement of antiferroelectric order. Further increasing La composition would enhance the stability of the antiferroelectric state at room temperature.[5] In addition, an incommensurate phase would be induced by doping of La, which has been observed using some typical techniques, such as hot-stage transmission electron microscopy (TEM), polarization electric-field (P-E) measurements characterized by Sawyer-Tower circuit, and dielectric spectroscopy.[6–10] Compared to parent compound PZT, incorporation of Sn^{4+} in the B-cation makes $Pb(Zr_{0.42}Sn_{0.40}Ti_{0.18})O_3$ (PZST) much easier in compositional tailoring.[11] Additionally, PZST lies very close to the MPB region given by Berlincourt,[12] which separates the antiferroelectric tetragonal and ferroelectric rhombohedral part of the phase diagram. Recently, we discovered a peculiar antiferroelectric phase in $(Pb_{1-1.5x}La_x)(Zr_{0.42}Sn_{0.40}Ti_{0.18})O_3$ (PLZST) ceramics, where the high-lying critical points present an abrupt variation with the temperature.[13] Note that the structure may be the incommensurate antiferroelectric phase. The phase transformations are associated with electronic transitions and electronic band structure variations, consequently resulting in the changes of interband critical points. Fortunately, Zhang *et al*. have explored an intrinsic relationship between optical band and phase transition for $Pb(Mg_{1/3}Nb_{2/3})O_3-xPbTiO_3$ single crystals.[4] Hence, it is an interesting issue for us to systematically investigate phase structure of PLZST ceramics through interband electronic transition variations.

It should be emphasized that spectroscopic ellipsometry (SE) is regarded as a highly appropriate method to determine dielectric functions of condensed matter materials over a wide energy and temperature range.[13–15] The dielectric function of a material is directly associated with its electronic band structure. Compared to electrical measurements, SE has many advantages, such as nondestructive measurement, two simultaneously measured dielectric function values ε_1 and ε_2 ($\varepsilon = \varepsilon_1 + i\varepsilon_2$), and better minimization of surface roughness. In this letter, the phase transformation and diagram have been investigated by temperature dependent SE. Moreover, the incommensurate antiferroelectric phase has been clearly observed and its origin can be discussed in detail.

The $(Pb_{1-1.5x}La_x)(Zr_{0.42}Sn_{0.40}Ti_{0.18})O_3$ (PLZST 100*x*/42/40/18) ceramics, where $x = 1.5\%$, 2.6%, 2.8%, and 3.4%, were fabricated by a conventional solid-state reaction sintering procedure. The details of fabricating process can be found in Ref. 5. Before spectral measurements, the ceramics were rigorously single-side polished and cleaned in pure ethanol with an ultrasonic bath and rinsed several times by deionized water. Temperature dependent SE data were collected from 1.1–6 eV (206–1100 nm) using a variable angle near-infrared-ultraviolet SE (J.A. Woollam Co., Inc.) with a fixed incident angle of 70°. The PLZST ceramics were

a)Author to whom correspondence should be addressed. Tel.: +86-21-54345150. Fax: +86-21-54345119. Electronic mail: zghu@ee.ecnu.edu.cn

mounted into an Instec cell with liquid nitrogen cooling accessory, in order to implement the temperature variation from 200 to 780 K with a precision of about ±1 K. The window effect can be eliminated through the calibration of silicon sample. The system was continuously purged with dry N_2 not only to protect the sample surface from contamination but also to avoid water vapor in the ambient.

The real part ε_1 and imaginary part ε_2 of the complex dielectric functions for PLZST ($x = 1.5\%$, 2.6%, 2.8%, and 3.4%) ceramics at 200, 300, 420, and 780 K are given in Fig. 1. In this work, the complex dielectric functions were derived from a three-layer model (air/surface roughness/ceramic). The surface roughness layer was modeled by Brüggeman effective-medium approximation (EMA) with a mixture of the bulk material (50%) and voids (50%). The thickness of the roughness layer can be fitted to about 6 nm from ellipsometric measurement, which agrees well with the data of the surface morphology by atomic force microscopy (AFM: Digital Instruments Icon, Bruker). The root-mean-square (RMS) surface roughness of PLZST ($x = 1.5\%$, 2.6%, 2.8%, and 3.4%) ceramics measured by AFM is estimated to about 5.99 nm, 5.52 nm, 4.52 nm, and 5.18 nm, respectively (not shown). Compared with the incident light spot of about 1 mm in diameter and grain size of about 42 nm, the scattering effects from the surface roughness layer and grain size can be neglected. Two parametric oscillators, including Psemi-M0 and Psemi-M3, were applied to estimate ε with WVASE32 software package (J.A. Woollam Co., Inc.). The ε spectra of all PLZST ceramics show the similar trend with increasing temperature. The imaginary part ε_2 is almost equal to zero below 3 eV (near the absorption edge) and increases sharply with increasing photon energy due to a strong optical absorption. With further increasing temperature, ε_2 passes through two interband critical point (CP) features, located at about 3.9 and 5.1 eV, labeled by arrows in Fig. 1. Moreover, the CP features from the spectra at 200 K are better resolved than those at 780 K. For example, the E_{cp2} feature at 5.0 eV is seen as a distinct peak in the ε_1 spectra at 200 K, while it appears as a weak shoulder at 780 K. It indicates that temperature has an obvious effect on the complex dielectric functions. Note that both of the CP energies in general show a red shift with increasing temperature, which can be attributed to the thermal expansion of the lattice and renormalization of the band structure by electron-phonon interaction.[16]

To obtain the accurate energies of CP structures and determine the temperature dependence, the second derivatives of the complex dielectric functions can be fitted by the standard critical point (SCP) model. The expression of SCP model is given by[17]

$$\frac{d^2\varepsilon}{dE^2} = \begin{cases} n(n-1)A_m e^{i\phi_m}(E - E_m + i\Gamma)^{n-2} & n \neq 0 \\ A_m e^{i\phi_m}(E - E_m + i\Gamma_m)^{-2} & n = 0, \end{cases} \quad (1)$$

where A_m is the amplitude, ϕ_m is the excitonic phase angle, E_m is the threshold energy, and Γ_m is the broadening parameter. The parameter m is the number of oscillators used in the fitting process. The exponent values $n = -1$, $-\frac{1}{2}$, 0, and $\frac{1}{2}$ represent excitonic one-, two-, and three-dimensional line shapes, respectively. In this work, the parameter n was set to -1. Both real and imaginary parts of the complex dielectric functions were fitted simultaneously. For example, the second derivatives of the complex dielectric functions spectra together with the best-fitting curves at 300 K are presented in Fig. 2(a). Compared to the complex dielectric functions, it shows that two distinct transitions can be readily distinguished due to minimizing the experimental noise. For comparison, the parameters of each composition at several temperatures are listed in Table I. The origins of the CP structures can be uniquely assigned as compared to the results from the density functional calculations.[18,19] The valence-band maximum (VBM) at X has the $X_{4'v}$ symmetry and consists of O p and Pb s states. The conduction-band minimum (CBM) is a mixture of O s and Pb p states at the X_{1c} symmetry. While the B ion d states contribute to the second conduction-band minimum at the X_{3c} symmetry. Thus,

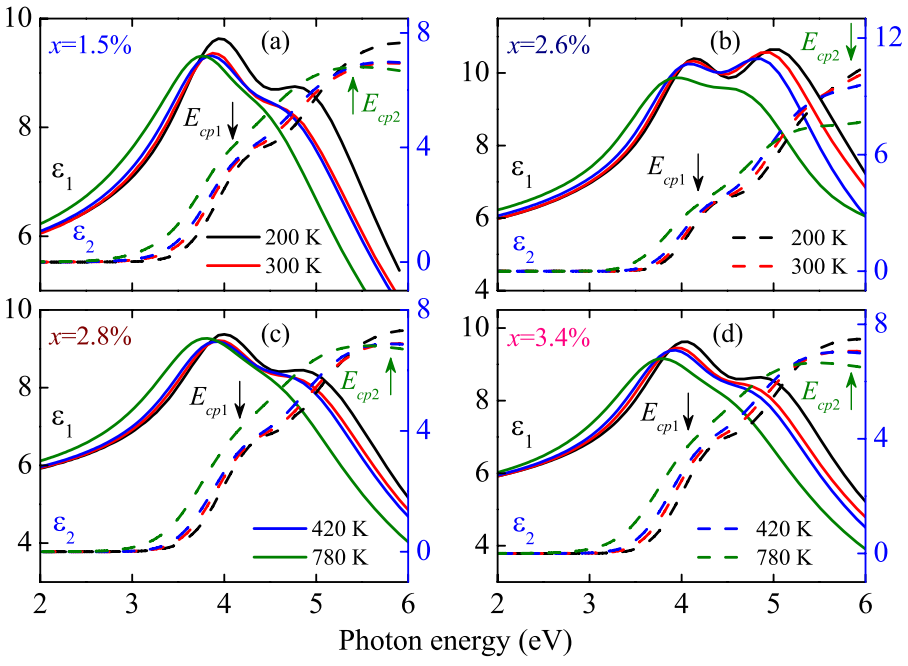

FIG. 1. The real part ε_1 (solid lines) and imaginary part ε_2 (dashed lines) of the complex dielectric functions for PLZST ceramics measured at 200, 300, 420, and 780 K, respectively. Two prominent interband CP features located at about 3.9 and 5.1 eV are indicated by the arrows.

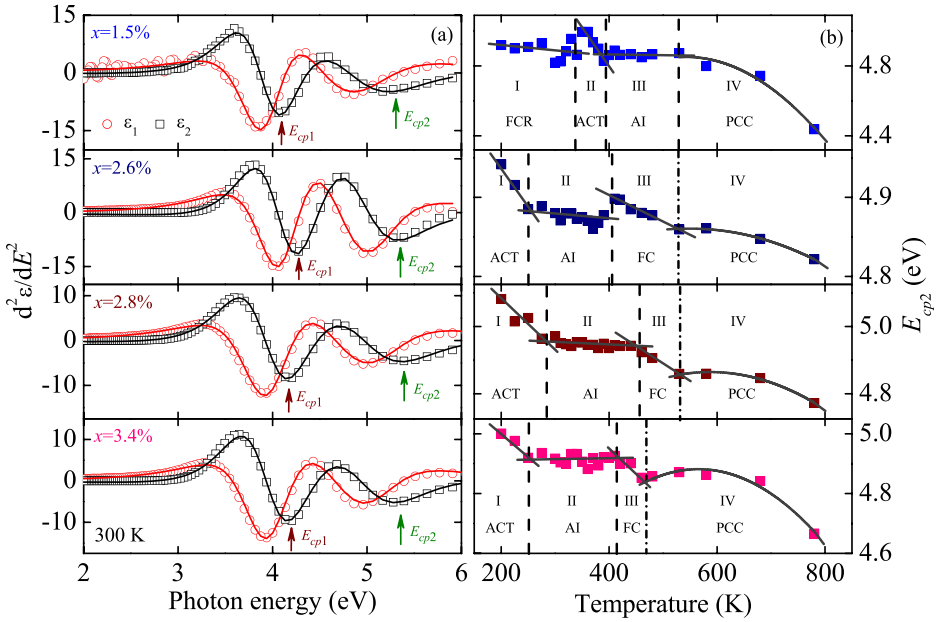

FIG. 2. (a) The second derivatives of the complex dielectric functions spectra (dotted lines) and the best-fitting curves (solid lines) at 300 K for PLZST ($x = 1.5\%$, 2.6%, 2.8%, and 3.4%) ceramics. The transition E_{cp1} and E_{cp2} features are indicated by the arrows. (b) Temperature dependence of the E_{cp2} energy for PLZST ceramics. The dashed lines show the boundaries of adjacent phases. The dashed-dotted lines are the borders of the ferroelectric cluster state and paraelectric commensurate cubic phase. Note that all CP energies are linearly and/or nonlinearly fitted with the solid lines to guide the eyes.

E_{cp1} is mostly attributed to the $X_{4'v} \rightarrow X_{1c}$ transition. As the $X_{4'v} \rightarrow X_{3c}$ transition is nearly forbidden, the transitions from the second valence band ($X_{5'v}$) to both conduction states X_{1c} and X_{3c} are responsible for E_{cp2} transition.

To elucidate the thermal evolution of interband electronic transitions, we plot the temperature dependence of E_{cp2} energy in Fig. 2(b). It should be emphasized that the transition E_{cp1} also presents the similar trend with the temperature from Table I. For PLZST with $x = 1.5\%$, the E_{cp2} transition can be divided into four parts: ferroelectric commensurate rhombohedral (FCR) phase, antiferroelectric commensurate tetragonal (ACT) phase, antiferroelectric incommensurate (AI) phase, and paraelectric commensurate cubic (PCC) phase. For PLZST ($x = 2.6\%$, $x = 2.8\%$, and $x = 3.4\%$), the interband transitions can be divided into three parts, including ACT, AI, and PCC phases, with ferroelectric cluster state (FC) existing in PCC phase. All of these energies generally show a red shift trend with the temperature, except for some particular regions, which is consistent with the above observation. The first three parts of each energy are linearly fitted. The temperature coefficients (about 10^{-4} eV/K order of magnitude) are typical values of perovskite materials.[13] However, the E_{cp2} energies of IV part (PCC phase) shows the nonlinear temperature dependence due to the decomposition of PbO_2 to Pb_3O_4.[13] In the PCC phase, an interesting feature is the presence of the ferroelectric cluster in the temperature region just above the AI phase for the PLZST ($x = 2.6\%$, 2.8%, and 3.4%) ceramics. It was reported that there is a slim-loop behavior in P-E curves, which indicates the presence of ferroelectric microdomains.[7] Note that the absolute values of temperature coefficients for II part of PLZST ($x = 1.5\%$) and III part of PLZST ($x = 2.6\%$, 2.8%, and 3.4%) are extremely small, showing an abrupt variation compared to other parts, which can be

TABLE I. Parameters of the SCP model for PLZST ($x = 1.5\%$, 2.6%, 2.8%, and 3.4%) ceramics extracted from the best fitting second derivatives of the complex dielectric functions at several temperatures. Note that the 95% reliability of the fitting parameters is given in parentheses.

Samples	$x = 1.5\%$			$x = 2.6\%$			$x = 2.8\%$			$x = 3.4\%$		
Temperature (K)	200	420	780	200	420	780	200	420	780	200	420	780
A_1	2.09	1.59	1.12	1.86	1.70	1.68	1.82	1.88	1.72	2.22	2.04	1.58
	(0.10)	(0.16)	(0.09)	(0.24)	(0.10)	(0.19)	(0.10)	(0.19)	(0.07)	(0.05)	(0.06)	(0.09)
ϕ_1 (deg)	20.9	20.8	21.4	20.7	20.6	20.5	21.0	20.7	20.6	20.7	20.6	20.8
	(0.03)	(0.05)	(0.01)	(0.10)	(0.07)	(0.04)	(0.04)	(0.08)	(0.03)	(0.05)	(0.03)	(0.05)
E_{cp1} (eV)	4.01	3.88	3.87	4.15	4.03	3.84	4.07	3.91	3.77	4.07	3.91	3.79
	(0.19)	(0.26)	(0.10)	(0.29)	(0.21)	(0.19)	(0.57)	(0.23)	(0.19)	(0.46)	(0.27)	(0.17)
Γ_1 (eV)	0.60	0.63	0.58	0.55	0.58	0.65	0.60	0.66	0.70	0.63	0.66	0.66
	(0.01)	(0.02)	(0.01)	(0.03)	(0.01)	(0.03)	(0.01)	(0.02)	(0.01)	(0.01)	(0.01)	(0.01)
A_2	3.39	3.95	6.15	3.63	3.48	2.86	4.57	3.57	4.29	2.85	2.83	4.23
	(0.59)	(0.64)	(0.36)	(0.76)	(0.35)	(0.23)	(0.47)	(0.06)	(0.24)	(0.22)	(0.17)	(0.28)
ϕ_2 (deg)	14.0	14.4	14.3	13.6	14.0	14.4	14.3	14.3	14.6	14.0	14.2	14.5
	(0.08)	(0.08)	(0.03)	(0.07)	(0.05)	(0.05)	(0.13)	(0.05)	(0.03)	(0.09)	(0.07)	(0.03)
E_{cp2} (eV)	4.92	4.86	4.44	4.94	4.89	4.83	5.08	4.95	4.76	5.00	4.89	4.68
	(0.03)	(0.02)	(0.02)	(0.03)	(0.01)	(0.02)	(0.04)	(0.01)	(0.01)	(0.01)	(0.03)	(0.01)
Γ_2 (eV)	0.87	1.08	1.21	0.81	0.80	0.86	1.05	1.01	1.19	0.82	0.91	1.15
	(0.04)	(0.05)	(0.04)	(0.08)	(0.04)	(0.04)	(0.05)	(0.03)	(0.03)	(0.03)	(0.02)	(0.05)

considered as the temperature independence of energies. The particular phenomenon can be ascribed to the appearance of AI phase. An incommensurate phase in the solid state is characterized by a modulated structure with an irrational period, in contrast to a commensurate phase whose period is rational.[20] Such incommensurate modulation has been observed in $PbZrO_3$ and $PbZrO_3$ based ferroelectric and antiferroelectric perovskite materials, using the selected area electron diffraction (SAED) technique in TEM.[7,10,21] As compared to the E_{cp1} transition, the E_{cp2} transition is more sensitive to the appearance of incommensurate antiferroelectric phase. The E_{cp2} transition is attributed to the combination of $X_{5'v} \rightarrow X_{1c}$ and $X_{5'v} \rightarrow X_{3c}$ transition, which is more relative to the composition of La than the E_{cp1} transition. However, the appearance of AI phase may be attributed to the modification of La. Thus, the E_{cp2} transition is more sensitive to the antiferroelectric incommensurate phase than the E_{cp1} transition.

To understand temperature dependence of the CP energies, we draw up the phase diagram of PLZST ceramics in Fig. 3. The phase diagram can be mainly divided into four parts, with FC state plotted with parallel lines in PCC phase. The AI phase exists between FC state and ACT phase, bordered with FCR phase. From the diagram, one can see that the substitution of La impurities for Pb ions leads to a conversion from ferroelectric rhombohedral phase to the antiferroelectric tetragonal phase at room temperature. With further increasing La composition to 2.6%, the antiferroelectric commensurate order becomes incommensurate. It indicates that the long-range ferroelectric coupling between dipoles is disrupted by La substitution and the short-range antiferroelectric coupling becomes dominant. This is in good agreement with x-ray diffraction (XRD) and spectral reflectance studies for the compositional sequence mentioned in our previous work.[5] It was reported that PLZST ceramic goes through a transformation from ferroelectric rhombohedral to antiferroelectric tetragonal phase when the composition of La exceeds 2.6%. For PLZST with $x = 2.8\%$, it is possible that PLZST ceramic has the coexistence of rhombohedral and tetragonal phases, of which the proportion of ferroelectric rhombohedral phase can be dominant. For PLZST with $x = 3.4\%$, however, it is clear that the ceramic is of single antiferroelectric tetragonal phase at room temperature. Thus, it is reasonable to predict a more stable antiferroelectric phase for PLZST system with more La doping.

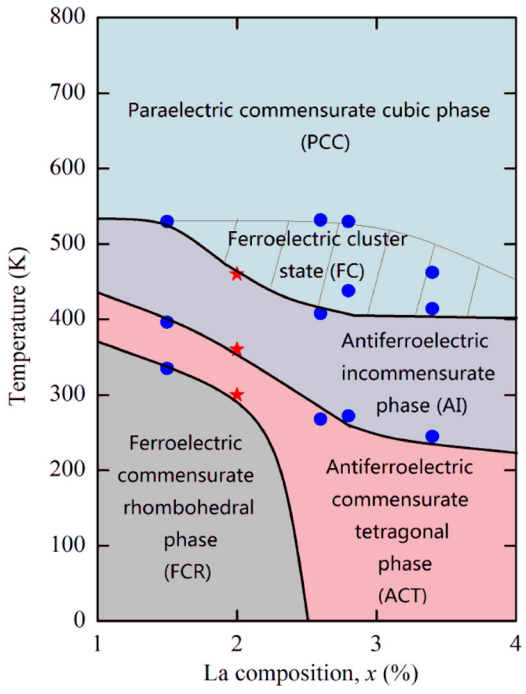

FIG. 3. The phase diagram of PLZST ceramics derived from the interband transition variations with the temperature and La composition. The phase transformation temperatures in the present work are marked with the solid circle dots and the star values are taken from Ref. 13. Reproduced with permission from Appl. Phys. Lett. **103**, 192910 (2013). Copyright 2013 by AIP Publishing LLC.

Furthermore, it is worth noticing that the samples undergo successive phase transitions as changing temperature. For PLZST with $x = 1.5\%$, when the temperature increases from the ferroelectric phase at 200 K, the ferroelectric to antiferroelectric phase transition happened on heating at about 340 K. On further heating, the antiferroelectric to paraelectric transformation was found to proceed through an incommensurate region. Meanwhile, with increasing La composition to 3.4%, it is found that the ACT phase was stabilized before room temperature and the transition sequence is ACT-AI-FC-PCC phase. Moreover, it shows that the temperature stability range of the AI phase becomes broadening and shifts to a lower temperature with increasing La compositions. It can be believed that the competition interactions between ferroelectric and antiferroelectric may lead to the appearance of the incommensurate phase. As mentioned before, the parent composition $Pb(Zr_{0.42}Sn_{0.40}Ti_{0.18})O_3$ lies very close to the MPB region, which separates the antiferroelectric tetragonal and the ferroelectric rhombohedral phase in the phase diagram. Thus, it could easily produce ferroelectric and antiferroelectric interactions and generate a rich phase picture by La modification. The origin of incommensurate antiferroelectric phase can be attributed to competition interactions favoring different structures. In addition, when La^{3+} ions substitute for Pb^{2+}, it could act as an impurity and may pin the incommensurate domain walls, favoring the formation of a metastable state.[22] Therefore, the temperature independence of CP energies in the incommensuration region can be explained by the pinning of incommensurate domain walls.[10,23] Note that the boundaries in the phase diagram should not be taken rigorously. It is because the phase coexistence may occur over a relatively wide temperature region.

To summarize, the thermal evolutions of PLZST ceramics have been investigated by temperature dependent spectroscopic ellipsometry. An incommensurate antiferroelectric phase was found and the phase diagram of PLZST ceramics has been well presented.

One of the authors (X. J. Ding) would like to thank Dr. Zhihua Duan, Dr. Xiao Chen, and Pengpeng Jiang for constructive discussion. This work was financially supported by Major State Basic Research Development Program of China (Grant Nos. 2011CB922200 and 2013CB922300), the Natural Science Foundation of China (Grant Nos. 11374097 and 61376129), Projects of Science and Technology

Commission of Shanghai Municipality (Grant Nos. 14XD1401500, 13JC1402100, and 13JC1404200), and the Program for Professor of Special Appointment (Eastern Scholar) at Shanghai Institutions of Higher Learning.

[1]A. S. Mischenko, Q. Zhang, J. F. Scott, R. W. Whatmore, and N. D. Mathur, Science **311**, 1270 (2006).
[2]G. H. Haertling, J. Am. Cream. Soc. **82**, 797 (1999).
[3]M. Ahart, M. Somayazulu, R. E. Cohen, P. Ganesh, P. Dera, H. K. Mao, R. J. Hemley, Y. Ren, P. Liermann, and Z. Wu, Nature **451**, 545 (2008).
[4]X. L. Zhang, Z. G. Hu, G. S. Xu, J. J. Zhu, Y. W. Li, Z. Q. Zhu, and J. H. Chu, Appl. Phys. Lett. **103**, 051902 (2013).
[5]X. Chen, K. Jiang, Z. G. Hu, X. F. Chen, G. S. Wang, X. L. Dong, and J. H. Chu, Appl. Phys. Lett. **101**, 011914 (2012).
[6]T. Asada and Y. Koyama, Phys. Rev. B **69**, 104108 (2004).
[7]Z. Xu, X. H. Dai, and D. Viehland, Phys. Rev. B **51**, 6261 (1995).
[8]I. MacLaren, R. Villaurrutia, and A. Peláiz-Barranco, J. Appl. Phys. **108**, 034109 (2010).
[9]J. Lee, J. Y. Yi, and K. S. Hong, J. Appl. Phys. **96**, 1174 (2004).
[10]Z. Xu, X. H. Dai, and D. Viehland, Appl. Phys. Lett. **65**, 3287 (1994).
[11]N. Luo, Y. Li, Z. Xia, and Q. Li, Cryst. Eng. Commun. **14**, 4547 (2012).
[12]D. Berlincourt, IEEE Trans. Sonics Ultrason. **13**, 116 (1966).
[13]X. Chen, P. P. Jiang, Z. H. Duan, Z. G. Hu, X. F. Chen, G. S. Wang, X. L. Dong, and J. H. Chu, Appl. Phys. Lett. **103**, 192910 (2013).
[14]S. G. Choi, R. Chen, C. Persson, T. J. Kim, S. Y. Hwang, Y. D. Kim, and L. M. Mansfield, Appl. Phys. Lett. **101**, 261903 (2012).
[15]S. G. Choi, J. Hu, L. S. Abdallah, M. Limpinsel, Y. N. Zhang, S. Zollner, R. Q. Wu, and M. Law, Phys. Rev. B **86**, 115207 (2012).
[16]H. Y. Fan, Phys. Rev. **82**, 900 (1951).
[17]P. Lautenschlager, M. Garriga, L. Vina, and M. Cardona, Phys. Rev. B **36**, 4821 (1987).
[18]H. Lee, Y. S. Kang, S. Cho, B. Xiao, H. Morkoç, T. D. Kang, G. S. Lee, J. Li, S. Wei, P. G. Snyder, and J. T. Evans, J. Appl. Phys. **98**, 094108 (2005).
[19]Z. Zhang, P. Wu, K. P. Ong, L. Lu, and C. Shu, Phys. Rev. B. **76**, 125102 (2007).
[20]P. Bak, Rep. Prog. Phys. **45**, 587 (1982).
[21]H. He and X. Tan, Phys. Rev. B **72**, 024102 (2005).
[22]K. Hamano, Y. Ikeda, T. Fujimoto, K. Ema, and S. Hirotsu, J. Phys. Soc. Jpn. **49**, 2278 (1980).
[23]W. Chan, Z. Xu, T. F. Hung, and H. Chen, J. Appl. Phys. **96**, 6606 (2004).